Noninvasive Detection of Tumor Hypoxia Using the 2-Nitroimidazole [^{18}F]EF1

Sydney M. Evans, Alexander V. Kachur, Chyng-Yann Shiue, Roland Hustinx, W. Timothy Jenkins, Grace G. Shive, Joel S. Karp, Abass Alavi, Edith M. Lord, William R. Dolbier, Jr., and Cameron J. Koch

Schools of Medicine and Veterinary Medicine, University of Pennsylvania, Philadelphia, Pennsylvania; Department of Chemistry, University of Florida, Gainesville, Florida; and the Cancer Center, University of Rochester, Rochester, New York

The noninvasive assessment of tumor hypoxia in vivo is under active investigation because hypoxia has been shown to be an important prognostic factor for therapy resistance. Various nuclear medicine imaging modalities are being used, including PET imaging of ^{18}F-containing compounds. In this study, we report the development of ^{18}F-labeled EF1 for noninvasive imaging of hypoxia. EF1 is a 3-monofluoro analog of the well-characterized hypoxia marker EF5, 2(2-nitro-1H-imidazol-1-yl)-N-(2,2,3,3,3-pentafluoropropyl)acetamide, which has been used to detect hypoxia in tumor and nontumor systems using immunohistochemical methods. **Methods:** We have studied 2 rat tumor types: the hypoxic Morris 7777 (Q7) hepatoma and the oxic 9LF glioma tumor, each grown in subcutaneous sites. PET studies were performed using a pharmacological dose of nonradioactive carrier in addition to [^{18}F]EF1 to optimize and assess drug biodistribution. After PET imaging of the tumor-bearing rats, tissues were obtained for γ-counting of the ^{18}F in various tissues and immunohistochemical detection of intracellular drug adducts in tumors. In one pair of tumors, Eppendorf needle electrode studies were performed. **Results:** [^{18}F]EF1 was excreted dominantly through the urinary tract. The tumor-to-muscle (T/M) ratio of [^{18}F]EF1 in the Q7 tumors was 2.7 and 2.4 based on PET studies and 2.1, 2.5, and 3.0 based on γ-counting of the tissues (n = 3). In contrast, the T/M ratio of [^{18}F]EF1 in the 9LF glioma tumor was 0.8 and 0.5 based on PET studies and 1.0, 1.2, and 1.4 based on γ-counting of the tissues (n = 3). Immunohistochemical analysis of drug adducts for the two tumor types agreed with the radioactivity analysis. In the Q7 tumor, substantial heterogeneous binding was observed throughout the tumor, whereas in the 9LF tumor minimal binding was found. **Conclusion:** [^{18}F]EF1 is an excellent radiotracer for noninvasive imaging of tumor hypoxia.

Key Words: hypoxia; tumor; PET; EF1; EF3; imaging; ^{18}F; rat; hepatoma; glioma

J Nucl Med 2000; 41:327–336

In recent years, understanding of the clinical and biologic significance of the tumor microenvironment has increased. The role of hypoxia in determining clinical outcome has been of particular interest. The observation that the presence of tumor cell hypoxia may be associated with a more aggressive biologic behavior (1,2) has initiated studies such as those by Reynolds et al. (3). Using a tumorigenic cell line carrying a recoverable, chromosomal-based λ-phage shuttle vector, exposure to hypoxia resulted in an elevated mutation frequency and a mutation pattern similar to that seen in hypoxic tumors (3). Hypoxia has been shown to upregulate gene products (4), which in turn have been associated with poor clinical prognosis. Clinically, tumor hypoxia has been associated with decreased local tumor control after radiation or surgery for cervical cancers (1), metastasis of high-grade extremity sarcomas (5), and local recurrence of head and neck cancers (2). In these studies, the presence of hypoxia has been determined using the Eppendorf needle electrode system. This system is somewhat limited in its general clinical application, primarily because of tissue access and the need for a very skilled operator to obtain and interpret the resulting pO$_2$ histograms. Two other clinically relevant techniques for assaying the presence of hypoxia are the comet assay (6) and the binding of 2-nitroimidazole drugs under hypoxic conditions (7–12). Assessment of the number and location of adducts formed by 2-nitroimidazole binding has been accomplished using immunohistochemistry (13) and nuclear medicine techniques (11). The primary advantage afforded by nuclear medicine techniques is their noninvasive nature. Noninvasive imaging of tumor hypoxia is currently being studied using either nuclear scintigraphy of iodine-labeled 2-nitroimidazoles, such as [^{131}I]IAZA (14), technetium-labeled molecules (15), or PET imaging of ^{18}F-labeled drugs such as fluoromisonidazole (FMISO) (11). The advantages of PET imaging over conventional scintigraphy techniques include the use of nanomolar doses of drug (lower dose of radioactivity) and better resolution. However, the short half-lives of the radionuclides used may limit the tumor-to-normal tissue true contrast in resulting images, as a result of insufficient clearance of nonspecifically bound drug.

EF5 has been studied extensively, using immunohistochemical detection of the reduced adducts in tissues. Monoclonal antibodies conjugated with fluorescent dyes have been reported and extensively characterized (8,13,16). Correlation of EF5 binding to several independent endpoints, including radiation response (7) and response to tirapaza-

mine and comet assay (*17*) have been made. In this study, we develop and present the PET imaging of [¹⁸F]EF1.

All drugs and precursors described in this study are derivatives of *N*-propyl-2-(2-nitroimidazol-1[H]-yl)-acetamide with 1 or more hydrogen atoms substituted by fluorine in the propyl group. The substitution occurs at the second and third carbon atoms (last 2 carbons of the propylamine sidechain). The name of each compound comprises the letter E (originally chosen to indicate that the side chains were similar to etanidazole), followed by the letter F (for fluorine), followed by 2 numbers separated by a comma (signifying the number of fluorine atoms on carbons 2 and 3, respectively). In cases in which the fluorine atoms are located only at the terminal carbon or in which there are no isomers, only a single number will be used (i.e., EF5 rather than EF2,3; EF3 rather than EF0,3; EF1 rather than EF0,1). Some precursors of the final drug are designated with a final "Br," indicating a bromine on carbon 3. For example, *N*-(3-bromo-propyl)-2-(2-nitroimidazol-1[H]-yl)-acetamide is named EFOBr. The common synthesis procedure has been to make halogen-substituted propylamine and then conjugate it to 2-nitroimidazole acetate as previously described for EF5 (*16*).

Two unique aspects of noninvasive hypoxic imaging with [¹⁸F]EF1 using PET are described. First, a new rationale regarding the importance and significance of drug half-life is presented. We suggest that it is not necessary to require rapid clearance of radioactive drug, as long as the drug biodistribution is uniform. Second, we present immunohistochemical studies of EF1 + EF3 drug binding to compare with the PET images. Both aspects are accomplished by administering the [¹⁸F]EF1 with unlabeled carrier (EF1) plus EF3 at whole-body drug levels of (30 + 100) μmol/L, respectively. Use of carrier drug in large excess over radioactive drug allows the independent assessment of drug biodistribution by conventional means (imaging, high-performance liquid chromatography [HPLC] determination) and, in addition, allows for immunohistochemical detection of intracellular EF1/EF3 adducts in the tumors using specific antibodies for EF3. The

correspondence of these analysis methods is presented in 2 rat tumor types, 1 of which is hypoxic (Morris 7777 hepatoma, Q7) and 1 of which is oxic (9LF glioma, 9LF).

MATERIALS AND METHODS

Drugs

Preparation of EF1 (Fig. 1) from 3-fluoropropylamine and 2-(2-nitroimidazol-1[H]-yl)-acetic acid, and [¹⁸F]EF1 from EFOBr and 2-(2-nitroimidazol-1[H]-yl)-acetic acid have been previously reported (*18*). Briefly, EF1 was prepared by conjugation of 3-fluoropropylamine with 2-(2-nitroimidazole-1[H]-yl)-acetic acid using the method of mixed anhydride with isobutylchloroformate (*16*). EFOBr was synthesized by an analogous method using 3-bromopropylamine. [¹⁸F]EF1 was prepared from EFOBr and potassium kryptofix [2.2.2] ¹⁸F in dimethyl sulfoxide (DMSO) at 120°C. A typical reaction mixture contained 1 mL DMSO, 10 μmol EFOBr (2.9 mg), 7 μmol of [KKrf]F, and 1.5 μmol potassium kryptofix carbonate ([KKrf]₂CO₃). The chemical yield of EF1 was up to 2% of the initial EFOBr. Purification was achieved by diluting the DMSO mixture with water and passing it through an anion exchange column. This simple method achieved up to 95% radiochemical purity, although clinical use would clearly require an additional purification by HPLC. The final specific activity of the EF1 used for injection was 5.6 × 10⁴ MBq/mol. This low specific activity was the result of the addition of nonradioactive fluoride (7 mmol/L) during [¹⁸F]EF1 synthesis and nonradioactive EF1 as carrier for injection. EF3 (Fig. 1) was synthesized by Dr. Mike Tracy (SRI International, Palo Alto, CA).

Tumor Models

Q7 cells were obtained from the American Type Culture Collection (Rockville, MD). They were maintained in exponential growth at 37°C by transfers at 3.5-d intervals. Growth medium was modified Eagle's medium supplemented with 15% fetal calf serum and standard penicillin and streptomycin. 9LF cells were obtained from Dr. Alan Franko (Cross Cancer Institute, Edmonton, Alberta, Canada). These cells have morphologic characteristics of 9L glioma tumors but, when grown in vivo in our laboratory, were radiation sensitive and bound minimal EF5 (Koch and Evans, unpublished data, 1995). They were maintained as described for Q7 cells, except that bovine calf serum was used as a media supplement.
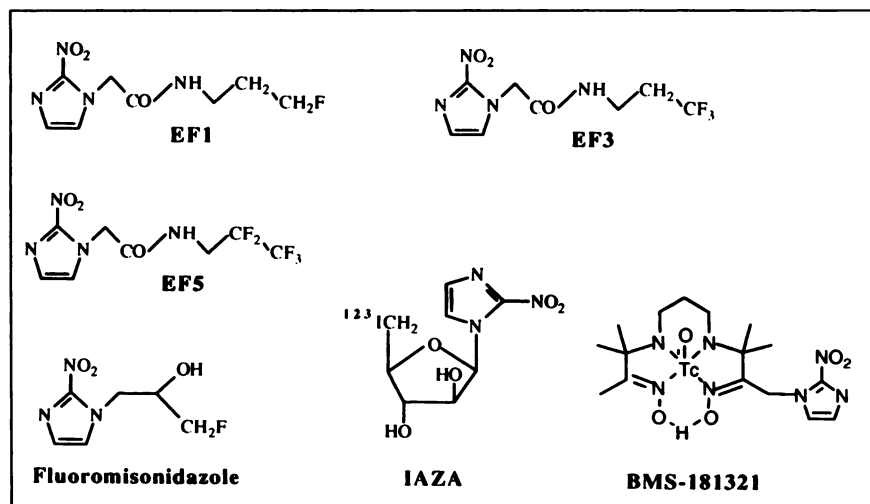

FIGURE 1. Chemical formulas of EF1, EF3, EF5, IAZA, FMISO, and BMS-181321.

All animal studies conformed to the regulations of the University of Pennsylvania Institutional Animal Care and Use Committee. For normal tissue biodistribution studies, 4–6-wk-old BALB/c nu/nu female mice were used. Male Buffalo rats (Harlan Sprague-Dawley, Indianapolis, IN) and male Fischer rats (Charles River, Wilmington, MA) were used for Q7 and 9LF studies, respectively. Tumors were produced by injecting 1 million tumor cells subcutaneously. The 9L tumor model takes 10–14 d to grow to a 1-cc tumor, and the Q7 tumor takes 14–20 d to grow to the same size.

In Vivo Studies

Two types of in vivo experiments were performed:

1. Nontumor-bearing mice: biodistribution (normal tissues and blood) of [18F]EF1
2. Tumor-bearing rat studies (6 animals total):

   a. PET imaging (n = 4)
   b. Biodistribution of [18F]EF1 in tumor, normal tissues, and blood (n = 6)
   c. Immunohistochemical detection of EF1/EF3 in tumor (n = 4)
   d. Eppendorf needle electrode studies (n = 2)

In 4 rats (3 9LF-bearing rats and 1 Q7-bearing rat), the bladder was exteriorized. This allowed for the bladder to be expressed preceding each image. This technique avoided the problem of high bladder activity dominating the camera's available response range. For PET imaging studies (total time, ~2.5 h), rodents were initially anesthetized with intraperitoneal ketamine (130 mg/kg) and xylazine (1.3 mg/kg), and anesthesia was maintained using additional smaller intraperitoneal injections of anesthetic, as needed. Drug was injected in a lateral tail or femoral vein; the total volume injected (in milliliters of physiological saline) was 1% of the animal's weight (in grams). The injection volume contained approximately 1.9 MBq [18F]EF1, 3 mmol/L carrier EF1, and 7 mmol/L EF3. Assuming an even biodistribution, the whole-body concentration of EF1 + EF3 was therefore 130 μmol/L. In one study of 2 rats, only 0.56 MBq [18F]EF1 could be synthesized, and the resulting PET studies were not interpretable because of poor counting statistics. After PET imaging studies, tumor, normal tissues, urine, and blood were removed, and the mass and radioactivity of a portion of each sample were determined. Tumor and liver were frozen for immunohistochemical analysis of EF3 biodistribution. EF3 was used as the dominant carrier, because it was expected that its biodistribution would be more similar to EF1 (because of increased polarity) than to EF5. Mice were injected with a proportionately smaller volume of drug mixture through the tail vein.

PET Imaging and Interpretation

The HEAD Penn-PET scanner (University of Pennsylvania, Philadelphia, PA) has a large axial extent, without septa, to achieve high sensitivity with 3-dimensional imaging techniques. Details regarding the scanner have been previously reported (19). Immediately before image reconstruction, the data were corrected for scatter and randoms. Image counts were collected for a 5-min interval at approximately 10, 30, 60, and 120 min after drug injection.

Regions of interest (ROIs) were manually drawn over the normal tissues and tumors. Similar regions were placed at the same level for each image. The activity within these ROIs was then measured and the values, in counts per second per voxel, were plotted against time. The kidneys could not be evaluated for 1 rat because high bowel (stomach) activity precluded reliably distinguishing the right kidney (data not shown). As noted earlier, ROIs could not be reliably drawn in 1 pair of rats because of poor counting statistics, and only the tissue γ-counts are included from these 2 animals.

Biodistribution Studies

At various times after drug injection, tissues, blood, and urine were collected. Each sample was weighed. The radioactivity of each sample was measured in a sodium iodide well counter (Gamma Counter 5000 Series; Packard Instrument Company, Downers Grove, IL), and the activity was expressed as a percentage injected dose per gram of sample. This value was calculated by comparison of the tissue counts to a known percentage of the injected activity, measured at the same time.

Tissue Preparation for Antibody Staining and Analysis of Sections

Tumor sections were cut at 14-μm thickness using a Microm HM 505N cryostat and collected onto poly-L-lysine–coated microscope slides. The sections were fixed for 1 h in ice-cold Dulbecco's phosphate-buffered saline (1X PBS) containing freshly dissolved paraformaldehyde (4%, pH 7.1–7.4, P-6148; Sigma Chemical Co., St. Louis, MO). The rinsing and blocking of tissue sections was identical to that described previously for EF5 (13). Monoclonal antibodies (designated ELK5-A8) made against EF3 tissue adducts were similar to those previously described for EF5 (16). These antibodies were conjugated with the green-excited, orange-emitting fluorescent dye, Cy3 (Amersham, Arlington Heights, IL).

EF3 binding was assessed by imaging the tissue sections at the appropriate wavelengths for Cy3. Slides were imaged using a Photometrics "Quantix" cooled CCD camera (Photometrics, Tucson, AZ), run by a Macintosh 9600 computer (Apple Computers, Inc., Cupertino, CA) and IP lab software (Scanalytics, Fairfax, VA). Sections were automatically scanned at constant camera exposure using a Ludl electronic stage, run by the same computer and software. Preceding microscope use, the brightness of the fluorescent bulb was calibrated so that the absolute brightness of the fluorescence could be determined. Cy3 dye with absorbency of 1.25 at 549 nm was loaded into a hemocytometer, and a fluorescence image was recorded after focusing the microscope on the ruled grid of the hemocytometer. Image fields of 1.05 × 0.7 mm were obtained for a 10× objective.

Eppendorf Needle Electrode Measurements

The Eppendorf needle electrode was calibrated by alternately bubbling N2 and air through the reference chamber and producing a calibration set before and after in vivo tumor measurements. A small portion of the skin overlying the tumor was removed to provide access for needle electrode insertion, and a scalpel blade was used to nick the capsular surface of the tumor. The electrode was advanced (typically 2–3 mm) through this opening until stable readings were observed. The needle progressed in 0.4-mm steps by advancing 0.7 mm followed by 0.3 mm withdrawal before the next measurement. pO2 values were normalized to pre- and postmeasurement calibrations.

RESULTS

Structures of drugs used in this study, as well as FMISO, IAZA, and BMS-181321, are shown in Figure 1.

The biodistribution of [^{18}F]EF1 with carrier EF1/EF3 was determined in 5 mice. Tissues were removed and counted in a γ-counter at 1 (n = 1), 5 (n = 2), and 90 (n = 2) min after injection. At 1 min, the radioactivity was in substantial disequilibrium, with higher specific activities in tissues with large fractional blood volumes (blood, liver, heart, muscle kidney, lung; data not shown). By 5 min, most nonexcretory tissue contained similar drug concentrations (Fig. 2A). An exception was brain, with about 10-fold reduced specific activity compared with other organs and tissues. [^{18}F]EF1 was excreted primarily through the urinary tract, as evidenced by the tremendous increase in urine counts by 90 min; at 5 min, the fractional activity per gram was negligible, whereas by 90 min it had increased to 0.6 (Fig. 2B). To a much lesser extent there was excretion through the gastrointestinal tract, as evidenced by increasing counts in the cecum. However, at 90 min, the fractional activity per gram was 20-fold higher in urine than in cecum. In all other tissues except bone (tibia), the radioactivity counts decreased substantially over time. Bone activity likely reflects contamination of the injectate by [^{18}F]F$^-$.
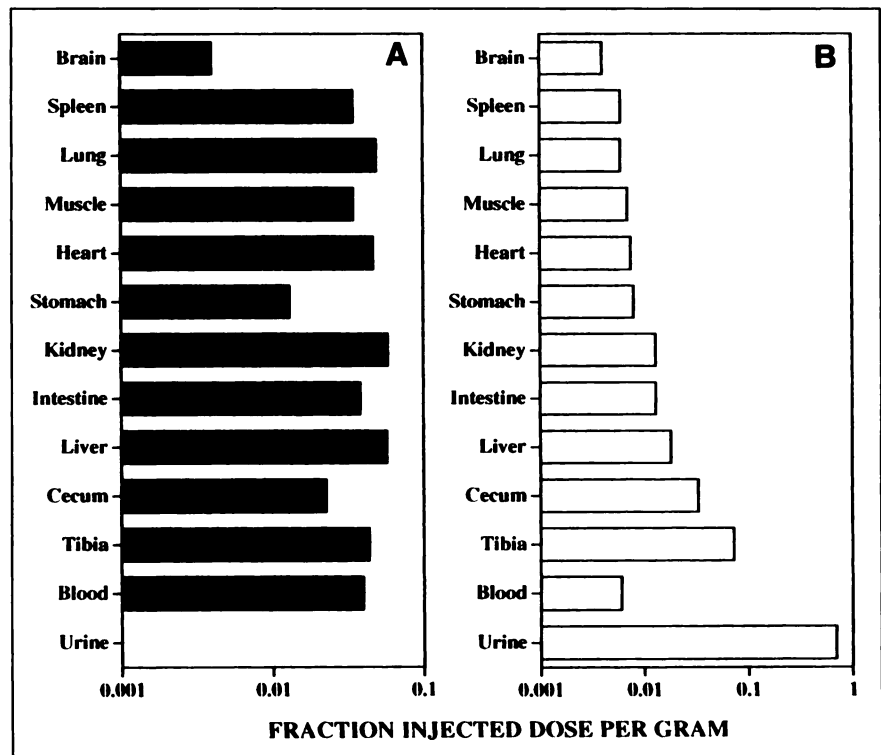
Transverse and sagittal images at the level of the tumor in 2 rats, 120 and 135 min after [^{18}F]EF1 injection, are presented in Figure 3. Figures 3A and B show the oxic 9LF tumor and Figures 3C and D show the hypoxic Q7 tumor. In Figures 3A and C, the 9LF tumor could not be discriminated from other tissue along the right body wall proximal to the kidney, despite presenting Figure 3C at maximal sensitivity. As a result of this high contrast, activity could be seen in the skeletal system (midline activity: spine).

At 120 min after injection, the Q7 tumor was easily seen

in the sagittal image on the rat's left body wall, adjacent to the region of the lung, diaphragm, and liver (Fig. 3C). High levels of activity could also be seen in the upper quadrant of the abdomen. These represented activity in the gastrointestinal tract (stomach) and kidney. In the transverse section through the midportion of the Q7 tumor (Fig. 3D), the only substantial activity was seen in the tumor. The only manipulation to the Q7 image was to collimate out bladder activity before analysis. This was necessary because of the very high urine activity (corrected in later experiments by exteriorizing the bladder; thus, the portion of the body presented in the sagittal image for the Q7 was shorter than that for the 9L). Similar findings were obtained in a second Q7-bearing rat, but the tumor was located in the subcutaneous tissues adjacent to the abdominal organs (data not shown). Differences in bowel retention between the 9LF and Q7-bearing rat were possibly attributable to differences in reagent preparation purity resulting in variations in route of excretion (e.g., almost entirely renal versus partially through the gastrointestinal tract) but may also have been caused by animal-to-animal variations, relative food intake, etc.

At the completion of the PET studies, tissues were removed from 2 Q7-bearing rats and 2 9LF-bearing rats and analyzed for radioactivity using γ-counting (Fig. 4). γ-count studies (Fig. 4A) support the data presented in Figure 2 for mice (e.g., high renal activity as a result of drug excretion). Irrespective of tumor type, activities in muscle, heart, spleen, and brain were similar and relatively low. Higher levels were present in the bone and Q7 tumor. Figure 4B presents the tumor-to-muscle (T/M) ratio of γ-counts for 6 rats (Q7 tumors: 2.1, 2.5, 3.0; 9LF tumors: 1.0, 1.2, 1.4).

FIGURE 2. Relative retention (fraction of injected activity/g) of radioactivity after injection of [^{18}F]EF1 into mice, with tissues collected at 5 (A) and 90 (B) min. With exception of brain, uptake was nearly equivalent for all but excretory tissues by 5 min (urine counts were not different from background). By 90 min, brain tissue was in equilibrium with blood and other low-binding tissues, and most radioactivity was now found in urine. Bone retention was likely caused by contaminating fluoride ion.
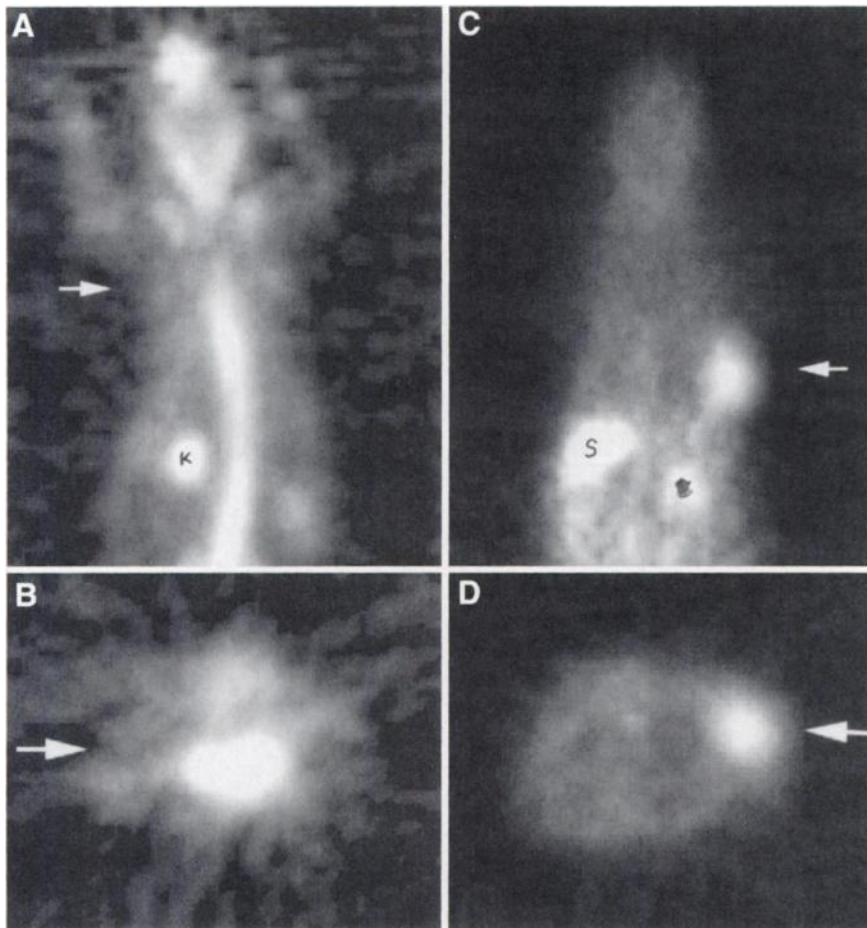
FRACTION INJECTED DOSE PER GRAM

FIGURE 3. Transverse and sagittal images in 2 tumor-bearing rats 120–135 min after [^{18}F]EF1 injection. (A) Sagittal image of rat bearing 9LF tumor adjacent to right thorax (arrow). (C) Transverse image of same animal at plane of tumor. Despite adjustment of camera sensitivity and contrast, tumor cannot be visualized adjacent to body wall on either image. (B) Sagittal image of rat bearing Q7 tumor (arrow). (D) Transverse image of same animal at plane of tumor (arrow). Note that tumor uptake is much higher than in any other tissue in plane. k = kidney; s = stomach.

PET images (e.g., Fig. 3) were analyzed to obtain time–activity curves for various tissues (Fig. 5). In all 4 rats studied, renal activity decreased over time (data not shown). There was no difference between the activity within the muscles, which were ipsilateral versus contralateral to the tumor, and these data were pooled. For Q7 tumors, the T/M activity ratios (Fig. 5A) initially decreased, then rose to a plateau. For 9L tumors, the T/M was constant with time (Fig. 5A). For the Q7 tumors, T/M ratios of 2.4 and 2.7 were achieved; in contrast, the T/M ratio for the 9LF tumors never exceeded 1. Similar conclusions arose from measuring absolute activity in each tumor versus time, normalized to the earliest time point (Fig. 5B). In the Q7 tumors, tumor activity decreased slightly over the first 50 min, then increased at 125 min, followed by a plateau. By contrast, in the 9LF tumors, there was a steady decrease in activity over time.

In 2 rats, 1 bearing a 9LF and 1 bearing a Q7 tumor, Eppendorf needle electrode studies were performed. In the Q7 tumor, the median pO_2 was 2.25 mm Hg and in the 9LF, 8.2 mm Hg. These data corresponded to the observation of a 2.5 (Q7) and 1.0 (9LF) T/M ratio using γ-counts.

After PET imaging, a portion of the tumor was frozen for sectioning and immunohistochemical staining with ELK5-A8 antibodies (specific against EF3 adducts; Lord and Koch, unpublished data, 1994) to corroborate the presence of

hypoxia in the PET imaged tumors (Fig. 6). A typical 1 × 0.7 mm region of one Q7 tumor is presented in the lower panel (Fig. 6B). Diffuse EF1/F3 binding was seen throughout the section. Regions of highest drug binding were adjacent to areas of cell death and necrosis. Nonbinding regions representing viable, aerobic cells were also seen. In contrast, there was a relative absence of binding in a 9LF tumor (Fig. 6A). Despite a camera exposure almost identical to that in Figure 6B (6 versus 6.5 s) only a few scattered regions with limited EF1/EF3 binding could be identified. Regions of necrosis were not identified in the 9LF tumor.

DISCUSSION

In recent years, there has been increasing interest in the diagnosis of hypoxia as a prognostic marker of disease. This interest has been intense in the field of oncology, in which hypoxia, based on Eppendorf electrode data, has been shown to predict tumor recurrence and metastasis (5). There are now preclinical and early clinical data supporting the use of antibody recognition of nitroimidazole adduct formation in tissues as a measure of hypoxia (13,20), and human clinical trials are underway (21). However, 1 limitation of this technique is the invasiveness of the assay (e.g., the requirement to obtain a tissue sample). In nononcologic diseases, such as myocardial infarction (22) or stroke, an invasive
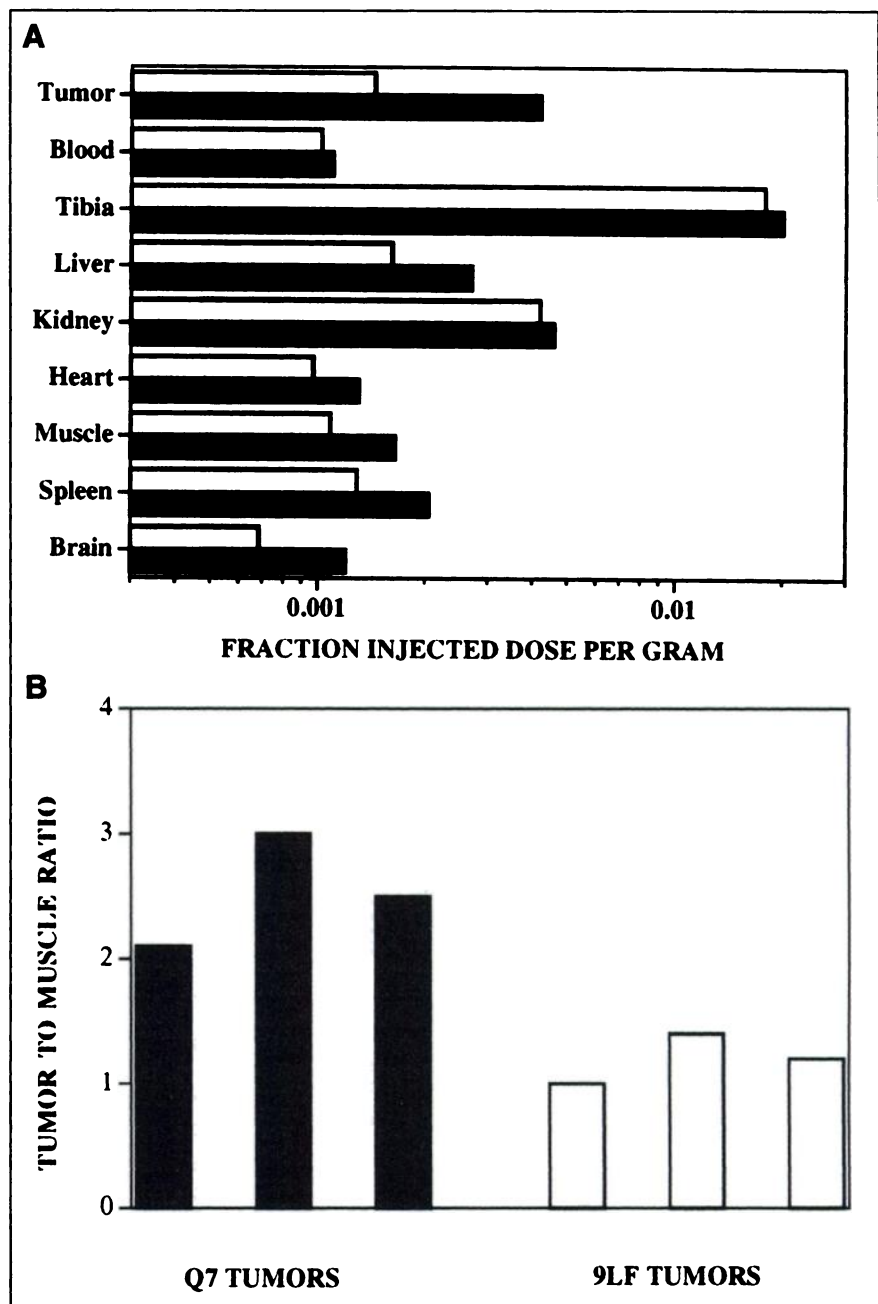
FIGURE 4. (A) γ-counts of tissues from tumor-bearing rats. High renal activity was the result of drug excretion. In 4 rats, irrespective of tumor type, heart, muscle, spleen, and brain levels were similar and relatively low. Higher levels were present in liver, kidney, and Q7 tumor. (B) T/M ratio for 3 Q7 tumors (black bars) and 3 9LF tumors (white bars).

assay would be contraindicated or impossible. Thus, several groups have been developing noninvasive assays to detect the distribution of hypoxic markers using nuclear medicine techniques. Examples include SPECT scanning of [131I]IAZA (23), nuclear medicine imaging of [99mTc]-labeled HL91 (24), and PET scans of [18F]FMISO (25,26). Thus far, several scientific and technical problems have been overcome, resulting in limited success. For the 131I-based techniques, whole-body radiation dose and deiodination (27) are problematic, but the available clinical data using 123I are encouraging (23,28). 99mTc-HL91 has been studied as both a tumor (24) and myocardial imaging agent (29). It is unclear from the data presented whether this drug represents a blood flow agent or truly images hypoxia. Ballinger et al. (30)

studied the 99mTc-labeled compound BMS181321 in vitro. Their studies suggest that this compound accumulates in both aerobic and hypoxic cells, with the latter being higher and time-dependent. For PET studies, clinical data have emphasized [18F]FMISO. This agent has been studied in several anatomic sites in humans, including gliomas (25), lung cancer (31), and nasopharyngeal carcinoma (26). Because picomolar drug concentrations were administered, drug biodistribution was difficult to assess. In addition, because of low tumor-to-normal tissue ratios, it was necessary to perform kinetic analyses to assess what has been termed "fractional hypoxic volumes" (31). FDG has also been studied from the perspective of imaging tumor metabolism, especially glucose. Minn et al. (32) have performed
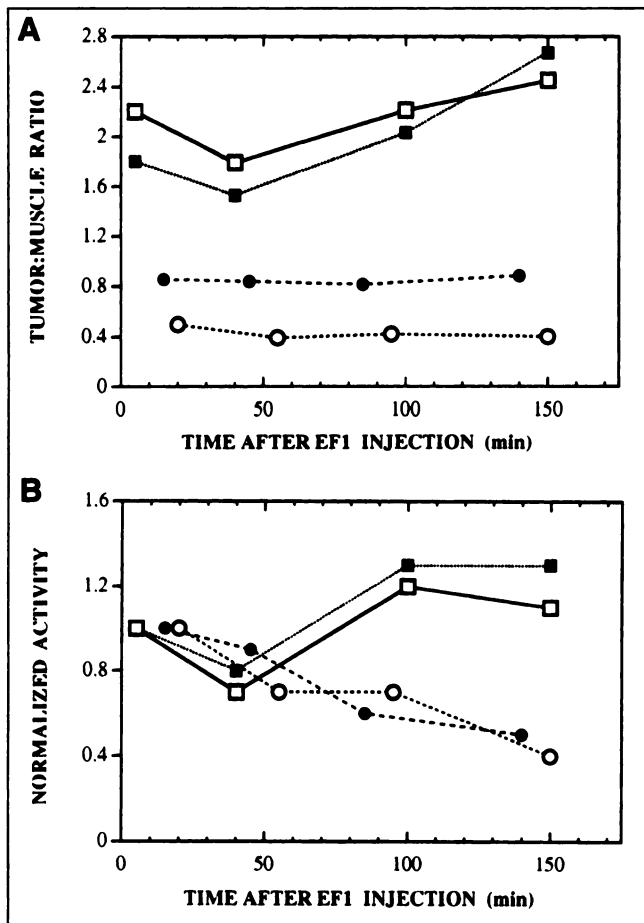
FIGURE 5. (A) For Q7 tumors, T/M activity ratios initially decreased, then rose to plateau (□,■). For 9L tumors, T/M was constant with time (O,●). For Q7 tumors, T/M ratios of 2.4 and 2.7 were achieved; in contrast, T/M ratio for 9LF tumors never exceeded 1. (B) Absolute activity in each tumor versus time, normalized to earliest time point. In Q7 tumors (□,■), tumor activity decreased slightly over first 50 min, then increased at 125 min followed by plateau. By contrast, in 9LF tumors (O,●), there was steady decrease in activity over time.

studies suggesting that FDG binding increases in the presence of hypoxia.

Herein we report biodistribution studies of [18F]EF1 in normal mice. Mice were chosen for this aspect of the study because of their small and consistent size and ease of handling tissues. Tumor and normal tissue studies were performed in 9LF-bearing Fischer rats and Q7-bearing Buffalo rats. These 2 tumor lines (and associated rat strains) were chosen because substantial data are available on tumor biology and physiology in these tumors, e.g., that 9LF tumors are predictably oxic and Q7 tumors are moderately hypoxic when the tumors are of moderate size (1–2 cm diameter, as used herein). Biodistribution of 2-nitroimidazole drugs has not been reported to be affected by rodent strain.

The results of investigations reported herein are unique, because the carrier drug (EF1/EF3) was used to a final whole-body concentration of 130 μmol/L. This technique

was used to avoid the problem of extremely small concentrations of radioactive drug being sequestered or metabolized before whole-body biodistribution occurred. Both EF1 and EF3 were added as components of the nonradioactive carrier. We have specific antibodies to EF5 and EF3, but not EF1. We chose EF3 rather than EF5 because the former is the more polar (and thus more similar to EF1). The resulting biodistribution data (Figs. 2 and 4) support the work of Laughlin et al. (33) using EF5 in mice (e.g., the drug distributes well to all organs and is excreted primarily through the urinary tract). One exception is that EF1, unlike EF5 (33), does not distribute optimally into the central nervous system, probably because it is much less lipophilic than EF5 (octanol: water partition coefficient, 1:5 versus 7:1, respectively). It has been argued that a polar drug is required to avoid neurotoxicity at high drug concentrations (34,35). In studies of EF5 in rodents (7,13), larger mammals (Koch and Evans, unpublished data, 1997), and in ongoing human studies, neurotoxicity with EF5 has not been found. Thus, development of an EF5-analog-based noninvasive assay of hypoxia is unlikely to be limited by neurotoxicity. However, our biodistribution data suggest that EF1 is too polar for optimal brain tissue access.

One of the most controversial aspects of the interpretation of nuclear medicine studies has been understanding exactly which physiological processes are being tracked. For example, FDG was originally developed to identify neoplastic cells based on their metabolic changes (e.g., atypical glucose metabolism) (36). Continuing studies on this agent have shown that its incorporation into cells is influenced by cell cycle (37), cell proliferative status (38), and hypoxia (32). Hypoxia would be expected only for cells showing a Pasteur effect (39). Similar questions regarding mechanism of activity have arisen with respect to labeled hypoxia imaging agents, because there has been no way to localize the agents independently and/or correlate their presence to an independent laboratory endpoint. Therefore, we set out to correlate 3 techniques to determine the biodistribution of injected drug: γ-counting and PET imaging for 18F, HPLC for parent drug, and immunohistochemistry for EF1/EF3 adducts. In the Q7-bearing rat shown in Figure 3A, for example, substantial binding is seen in PET images of the tumor at 135 min, especially compared with adjacent muscle. Analysis of these images result in a T/M ratio of 2.5 (Fig. 5B). γ-counts from these tissues demonstrate a T/M ratio of 3.0 (Fig. 4). Immunohistochemical analysis of the tumor tissue shows moderate binding of EF1/EF3 in hypoxic regions adjacent to regions of necrosis and distant from vessels (Fig. 6B). Conversely, in the 9LF tumor, the T/M ratio based on γ-counts was 1.4 and that based on time–activity curves was 0.8. In the immunohistochemical images, only a few small regions of EF1/EF3 binding were seen. These data, especially in light of previous work on EF5 (7,8,13), are highly supportive of the concept that late PET images of [18F]EF1 represent tumor hypoxia. Early uptake in the time course (5 min) for the Q7 tumors likely represents perfusion-related effects.
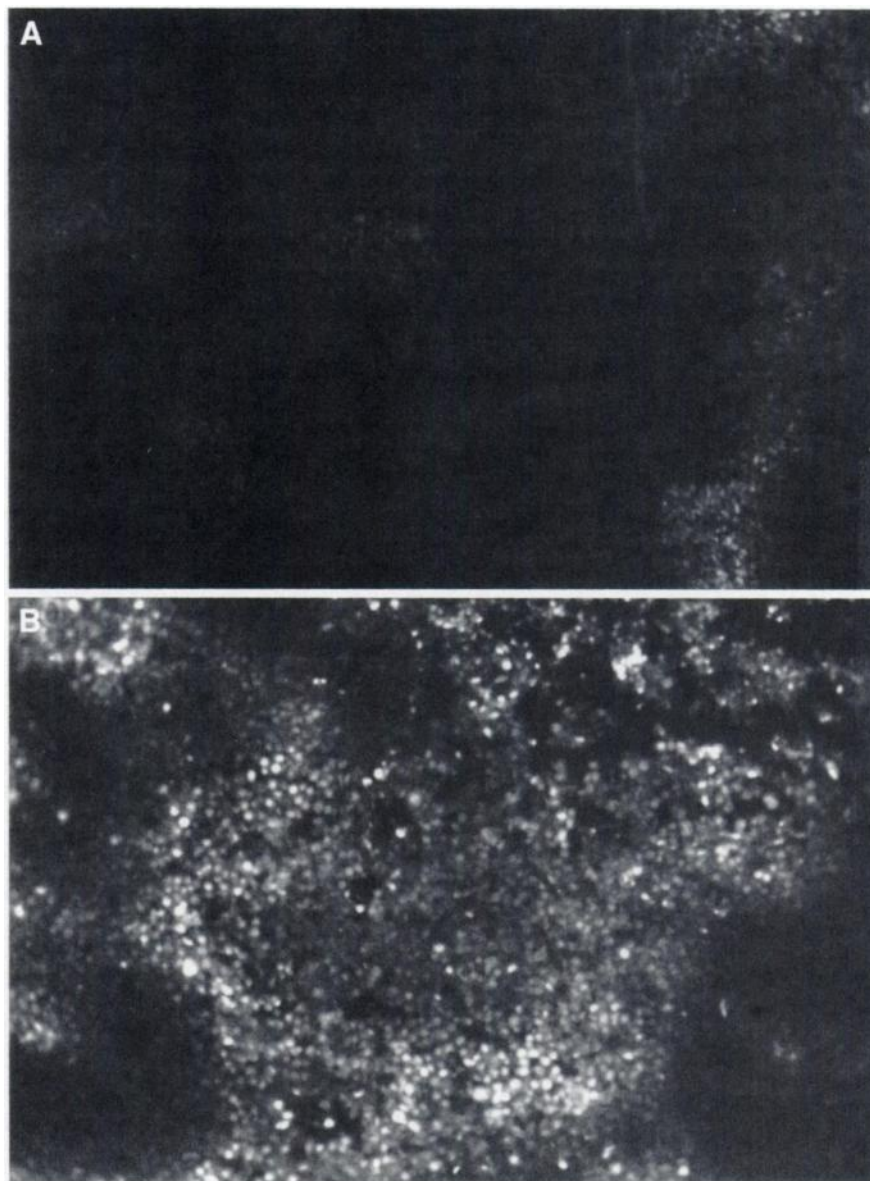
FIGURE 6. Immunohistochemical analysis of EF3 binding in Q7 (B) versus 9L (A) tumor tissue; each panel illustrates typical 1.0 × 0.7 mm area. Diffuse EF1/F3 binding is seen throughout Q7 section. Regions of highest drug binding were seen adjacent to areas of necrosis. Nonbinding regions representing viable, aerobic cells are also seen. Note relative absence of binding in 9LF tumor (A). Despite camera exposure almost identical to that in B (6 versus 6.5 s), only scattered regions of limited EF1/EF3 binding can be identified. For both images, pixel intensity has been increased by factor of 3 to improve visibility of binding in 9LF tumor. No alterations in background or contrast were made.

Wiebe and Stypinski (40) provided an excellent review of the importance of the pharmacokinetic characterization of radiopharmaceuticals, with emphasis on those that are being developed for imaging hypoxia. They have characterized the ideal hypoxia pharmaceutical in the following way: "[it] must concentrate efficiently and selectively in target cells, while keeping the radiation dose to the patient within acceptable levels. The radiopharmaceutical must be cleared quickly from the blood to minimize radioactivity to produce a clear image of the (hypoxic) tissue in the patient. Perhaps the most important requirement is that it must have a mean residence time long enough to allow it to diffuse into the hypoxic areas, which are regions of diminished blood supply." In further discussion, they note that "ideally, 100% of the dose should be eliminated renally" and that "to accurately interpret the results of an imaging study, the intracellular uptake must be detailed along with overall biodistribution" (40). Some of these desirable properties may be incompatible. Rapid renal clearance is typically associated with highly polar compounds, and such compounds are known to have quite heterogeneous whole-body distributions, with particular emphasis on exclusion from the central nervous system and other neural tissues. Even with dominant renal clearance, drug half-lives will increase substantially in humans compared with the smaller animals used in preclinical studies. This can be problematic when radioactive isotopes are used, since the half-lives of the isotopes are fixed. Thus, it has been suggested that noninvasive hypoxia assays using PET will always suffer from the very short half-lives of the available isotopes (14). Not mentioned in this and other reviews (14,40) is the potential problem of drug availability in vivo. Many nitroimidazoles are known to fragment to other molecules, which may or may not have the desired labeling characteristics. This problem is further exacerbated by the chemical stability of the isotope–drug linkage, with halogens other than fluorine

being particularly susceptible to metabolism, exchange, or hepatic elimination. The pharmacokinetic analyses of the drugs used in nuclear medicine assays often have created uncertainties because of the low drug concentrations used and because assays are limited to detection of the associated radioactive atom. This problem is paramount with technetium, because stable isotopes are not available.

In light of the preceding discussion, we believe that our approach to noninvasive assays of hypoxia differs in 3 primary ways from previous studies:

1. In vivo drug stability of EF1 and its analogs is exceptionally high. This extends, as with other fluorinated compounds, to the stability of the bound isotope.
2. Use of high carrier drug concentrations allows assessment of the biodistribution of drug and its metabolites by conventional (immunohistochemical) and HPLC-based assays, in addition to radioactive assays.
3. High drug concentrations and reduced polarity will result in a longer drug half-life than isotope half-life. Thus, we suggest emphasizing a uniform drug biodistribution. Imaging thus entails differentiating metabolism-induced increases on a constant background of non-metabolized drug, possibly complicated by perfusion artifacts at early times (14).

The results provided herein demonstrate that EF1 provides many of the advantageous characteristics of a PET molecule with few of the problematic ones. We clearly demonstrate that PET imaging with [18F]EF1 is able to differentiate hypoxic versus aerobic tumors in rodents. The high T/M ratio seen in the hypoxic Q7 tumors allows an easy delineation of the lesion without complex image or kinetic analyses. Our ongoing work is directed at further developing drugs in the EF1– EF5 series for PET imaging. This study will emphasize increasing lipophilicity through multiple fluorinated sites, such as [18F]EF3 and [18F]EF5, while maintaining pharmacologic concentrations (up to 100 μmol/L) of nonradioactive drug.

ACKNOWLEDGMENTS

REFERENCES

1. Hockel M, Schlenger K, Aral B, Mitze M, Schaffer U, Vaupel P. Association between tumor hypoxia and malignant progression in advanced cancer of the uterine cervix. Cancer Res. 1996;56:4509–4515.
2. Brizel DM, Sibley GS, Prosnitz LR, Scher RL, Dewhirst MW. Tumor hypoxia adversely affects the prognosis of carcinoma of the head and neck. Int J Radiat Oncol Biol Phys. 1997;38:285–289.
3. Reynolds TY, Rockwell S, Glazer PM. Genetic instability induced by the tumor microenvironment. Cancer Res. 1996;56:5754–5757.
4. Waleh N, Brody M, Knapp M, et al. Mapping of the vascular endothelial growth factor-producing hypoxic cells in multicellular tumor spheroids using a hypoxia-specific marker. Cancer Res. 1995;55:6222–6226.
5. Brizel DM, Scully SP, Harrelson JM, et al. Tumor oxygenation predicts for the likelihood of distant metastases in human soft tissue sarcoma. Cancer Res. 1996;56:941–943.
6. Olive PL, Durand RE, LeRiche J, Jackson SM. Gel electrophoresis of individual cells to quantify hypoxic fraction in human breast cancers. Cancer Res. 1993;53:733–736.
7. Evans SM, Jenkins WT, Joiner B, Lord EM, Koch CJ. 2-Nitroimidazole (EF5) binding predicts radiation resistance in individual 9L s.c. tumors. Cancer Res. 1996;56:405–411.
8. Koch CJ, Evans SM, Lord EM. Oxygen dependence of cellular uptake of EF5 [2-(2-nitro-1H-imidazol-1-yl)-N-(2,2,3,3,3-pentafluoropropyl)acetamide]: analysis of drug adducts by fluorescent antibodies vs bound radioactivity. Br J Cancer. 1995;72:869–874.
9. Hodgkiss RJ, Jones G, Long A, et al. Flow cytometric evaluation of hypoxic cells in solid experimental tumours using fluorescence immunodetection. Br J Cancer. 1991;63:119–125.
10. Raleigh JA, Miller GG, Franko AJ, Koch CJ, Fuciarelli AF, Kelley DA. Fluorescence immunohistochemical detection of hypoxic cells in spheroids and tumours. Br J Cancer. 1987;56:395–400.
11. Rasey JS, Grunbaum Z, Magee S, et al. Characterization of radiolabeled fluoromisonidazole as a probe for hypoxic cells. Radiat Res. 1987;111:292–304.
12. Varghese AJ, Gulyas S, Mohindra JK. Hypoxia-dependent reduction of 1-(2-nitro-1-imidazolyl)-3-methoxy-2-propanol by Chinese hamster ovary cells and KHT tumor cells in vitro and in vivo. Cancer Res. 1976;36:3761–3765.
13. Evans SM, Joiner B, Jenkins WT, Laughlin KM, Lord EM, Koch CJ. Identification of hypoxia in cells and tissues of epigastric 9L rat glioma using EF5 [2-(2-nitro-1H-imidazol-1-yl)-N-(2,2,3,3,3-pentafluoropropyl) acetamide]. Br J Cancer. 1995;72:875–882.
14. Chapman JD, Engelhardt EL, Stobbe CC, Schneider RF, Hanks GE. Measuring hypoxia and predicting tumor radioresistance with nuclear medicine assays. Radiother Oncol. 1998;46:229–237.
15. Linder K, Chan Y, Cyr J, Malley M, Nowotnik D, Nunn A. TcO(PnA-O-1-(2-nitroimidazxole)) [BMS-181321] a new technetium-containing nitroimidazole complex for imaging hypoxia: synthesis, characterization, and xanthine oxidase catalyzed reduction. J Med Chem. 1994;37:9–17.
16. Lord EM, Harwell L, Koch CJ. Detection of hypoxic cells by monoclonal antibody-recognizing 2-nitroimidazole adducts. Cancer Res. 1993;53:5271–5276.
17. Brown JM, Giaccia AJ. The unique physiology of solid tumors: opportunities (and problems) for cancer therapy. Cancer Res. 1998;58:1408–1416.
18. Kachur A, Evans SM, Shive C-Y, et al. Synthesis of new hypoxia markers EF1 and [18F]-EF1. Appl Radiat Isot. 1999;51:643–650.
19. Karp JS, Freifelder R, Geagan MJ, et al. Three-dimensional imaging characteristics of the HEAD PENN-PET scanner. J Nucl Med. 1997;38:636–643.
20. Cline JM, Thrall DE, Page RL, Franko AJ, Raleigh JA. Immunohistochemical detection of a hypoxia marker in spontaneous canine tumours. Br J Cancer. 1990;62:925–931.
21. Raleigh JA, Calkins-Adams DP, Rinker LH, et al. Hypoxia and VEGF expression in human squamous cell carcinomas using pimonidazole as a hypoxia marker. Cancer Res. 1998;58:3765–3768.
22. Bialik S, Greenen DL, Sasson IE, et al. Myocyte apoptosis during acute myocardial infarction in the mouse localizes to hypoxic regions but occurs independently of p53. J Clin Invest. 1997;100:1363–1372.
23. Parliament MB, Chapman JD, Urtasun RC, et al. Non-invasive assessment of human tumour hypoxia with 123I-iodoazomycin arabinoside: preliminary report of a clinical study. Br J Cancer. 1992;65:90–95.
24. Cook GJ, Houston S, Barrington SF, Fogelman I. Technetium-99m-labeled HL91 to identify tumor hypoxia: correlation with fluorine-18-FDG. J Nucl Med. 1998;39:99–103.
25. Valk PE, Mathis CA, Prados MD, Gilbert JC, Budinger TF. Hypoxia in human gliomas: demonstration by PET with fluorine-18-fluoromisonidazole. J Nucl Med. 1992;33:2133–2137.
26. Yeh SH, Liu RS, Wu LC, et al. Fluorine-18 fluoromisonidazole tumour to muscle retention ratio for the detection of hypoxia in nasopharyngeal carcinoma. Eur J Nucl Med. 1996;23:1378–1383.
27. Cherif A, Wallace S, Yang DJ, et al. Development of new markers for hypoxic cells: [131I]iodomisonidazole and [131I]iodoerythronitroimidazole. J Drug Target. 1996;4:31–39.
28. Groshar D, McEwan AJ, Parliament MB, et al. Imaging tumor hypoxia and tumor perfusion. J Nucl Med. 1993;34:885–888.
29. Okada RD, Johnson G III, Nguyen KN, Edwards B, Archer CM, Kelly JD. 99mTc-HL91. Effects of low flow and hypoxia on a new ischemia-avid myocardial imaging agent. Circulation. 1997;95:1892–1899.
30. Ballinger JR, Kee JW, Rauth AM. In vitro and in vivo evaluation of a technetium-99m-labeled 2-nitroimidazole (BMS181321) as a marker of tumor hypoxia. J Nucl Med. 1996;37:1023–1031.

31. Koh WJ, Bergman KS, Rasey JS, et al. Evaluation of oxygenation status during fractionated radiotherapy in human nonsmall cell lung cancers using [F-18]fluoromisonidazole positron emission tomography. *Int J Radiat Oncol Biol Phys.* 1995;33:391–398.

32. Minn H, Clavo AC, Wahl RL. Influence of hypoxia on tracer accumulation in squamous-cell carcinoma: in vitro evaluation for PET imaging. *Nucl Med Biol.* 1996;23:941–946.

33. Laughlin KM, Evans SM, Jenkins WT, et al. Biodistribution of the nitroimidazole EF5 (2-[2-nitro-1H-imidazol-1-yl]-N-(2,2,3,3,3-pentafluoropropyl) acetamide) in mice bearing subcutaneous EMT6 tumors. *J Pharmacol Exp Ther.* 1996;277:1049–1057.

34. Aboagye EO, Lewis AD, Graham MA, et al. The pharmacokinetics, bioavailability and biodistribution in mice of a rationally designed 2-nitroimidazole hypoxia probe SR-4554. *Anticancer Drug Des.* 1996;11:231–242.

35. Brown JM, Yu NY, Brown DM, Lee WW. SR-2508: a 2-nitroimidazole amide which should be superior to misonidazole as a radiosensitizer for clinical use. *Int J Radiat Oncol Biol Phys.* 1981;7:695–703.

36. Wahl RL, Hutchins GD, Buchsbaum DJ, Liebert M, Grossman HB, Fisher S. 18F-2-deoxy-2-fluoro-D-glucose uptake into human tumor xenografts: feasibility studies for cancer imaging with positron-emission tomography. *Cancer.* 1991;67:1544–1550.

37. Kubota R, Kubota K, Yamada S, Tada M, Ido T, Tamahashi N. Active and passive mechanisms of [fluorine-18] fluorodeoxyglucose uptake by proliferating and prenecrotic cancer cells in vivo: a microautoradiographic study. *J Nucl Med.* 1994;35:1067–1075.

38. Slosman DO, Pittet N, Donath A, Polla BS. Fluorodeoxyglucose cell incorporation as an index of cell proliferation: evaluation of accuracy in cell culture. *Eur J Nucl Med.* 1993;20:1084–1088.

39. Koch CJ, Giandomenico AR, Iyengar CW. Bioreductive metabolism of AF-2[2-(2-furyl)-3-(5-nitro-2-furyl)acrylamide] combined with 2-nitroimidazoles: implications for use as hypoxic cell markers. *Biochem Pharmacol.* 1993;46:1029–1036.

40. Wiebe LI, Stypinski D. Pharmacokinetics of SPECT radiopharmaceuticals for imaging hypoxic tissues. *Q J Nucl Med.* 1996;40:270–284.